Age-Related Changes in Quantitative Strain of Mouse Astrocytic Lamina Cribrosa and Peripapillary Sclera Using Confocal Microscopy in an Explant Model

Cathy Nguyen, Dan Midgett, Elizabeth Kimball, Joan Jefferys, Thao D. Nguyen, Julie Schaub, Mary Pease, and Harry Quigley

The Glaucoma Center of Excellence, Wilmer Ophthalmological Institute and the Department of Mechanical Engineering, Johns Hopkins University, Baltimore, Maryland, United States

Correspondence: Harry Quigley, Wilmer Eye Institute 122, Johns Hopkins Hospital, 600 North Broadway, Baltimore, MD 21287, USA; hquigley@jhmi.edu.

Submitted: June 21, 2018
Accepted: September 9, 2018

Citation: Nguyen C, Midgett D, Kimball E, et al. Age-related changes in quantitative strain of mouse astrocytic lamina cribrosa and peripapillary sclera using confocal microscopy in an explant model. *Invest Ophthalmol Vis Sci*. 2018;59:5157–5166. https://doi.org/10.1167/iovs.18-25111

Purpose. The purpose of this study was to measure the full-field deformation response to IOP change in the peripapillary sclera (PPS) and astrocytic lamina cribrosa (ALC) of young and old mouse eyes ex vivo.

Methods. Thirty-eight transgenic reporter mice with green fluorescent protein–expressing astrocytes were studied at 2 to 4 months and 13 to 15 months old. The ALC and PPS of the explant eyes were imaged using laser scanning microscopy under controlled inflation from 10 to 30 mm Hg. Strains were estimated for the ALC and PPS from imaged volumes using digital volume correlation.

Results. ALC strains were significantly greater than zero nasal–temporally for both age groups (mean = 4.3% and 4.0%; each $P \leq 0.004$) and significantly greater than zero in the inferior–superior direction for younger mice ($P = 0.0004$). Younger mice had larger ALC inferior–superior strains than older mice ($P = 0.002$). The ALC area and perimeter enlarged with inflation in both age groups, with a greater increase in younger than in older mice (all $P \leq 0.004$). The ALC nasal–temporal diameter change was greater than inferior–superiorly, and younger mice had greater enlargement nasal–temporally than older. PPS maximum shear strain was greater in the older mice ($P = 0.002$). The axial lengths of older mice were 14% longer and the PPS was 16% thinner than younger mice (both $P = 0.0003$).

Conclusions. The behavior of the ALC in younger mice with inflation exhibited greater strains and enlargement of ALC area than older mice. Some strain measures in the PPS were greater in older mice, likely related to their longer axial length and thinner PPS.

Keywords: glaucoma, sclera, optic nerve head, mouse, astrocyte, retinal ganglion cell, extracellular matrix, collagen

Glaucoma is characterized by damage to the retinal ganglion cell axons and their cell bodies. In human open angle glaucoma, the level of IOP is a consistent risk factor, with stress related to IOP being associated with ganglion cell damage in a substantial number of affected eyes at normal levels of IOP.[1] The effect of IOP on ganglion cells, whether at lower or higher IOP levels, is thought to act by its effect on ocular supportive tissues in the peripapillary sclera (PPS) and optic nerve head (ONH). IOP deforms the neural and connective tissues of the ONH through both a translaminar pressure gradient and tensile stresses in the peripapillary sclera (PPS). Recent studies of the lamina cribrosa (LC) and PPS from postmortem human eyes confirmed that zones of lower connective tissue density in the LC are associated with greater strain and correspond to the specific areas of greater ganglion cell axon loss (Ling YTT, et al. *IOVS* 2018; 213:ARVO E-Abstract 1219). This regional susceptibility corresponds to the typical pattern of visual field loss in glaucoma.[2] The biomechanical responses of human eyes in vivo differ in normal and glaucoma eyes and differ between damaged and undamaged regions of the LC.[3] Numerous theoretical reviews of this area and ex vivo studies have used data from postmortem human and experimental monkey eyes to propose analytic approaches to these issues, but direct measurements of actual tissue responses are more difficult to generate. Thus, measurements in animal models of ONH tissues can contribute to this research area.

Experimental models of glaucoma in the mouse, rat, and monkey all produce interruption of ganglion cell axonal transport at the ONH, as it occurs in human glaucoma. Sun et al.[4] demonstrated that ganglion cell axons pass through a set of pores formed from processes of astrocytes that stretch from one side of the nerve head to the other, perpendicular to the axons. This entirely cellular configuration is strikingly similar to that of the mammalian nerve head, which has connective tissue–containing beams lined by astrocytes passing across the nerve head.[5] Likewise, the PPS of the mouse eye contains a zone of circumferentially aligned collagen and elastin fibers, which is quite similar to that found in the human PPS, which allows this zone in both species to resist circumferential expansion. The study of similarities and differences in the biomechanical behavior of mouse and human eyes could enhance our understanding of the mechanisms that translate IOP elevations into glaucomatous optic nerve damage. The present investigation studies acute IOP-generated changes in

mouse eyes at two specified age ranges. Indeed, using chronic IOP elevation, we and others have determined that substantial remodeling and cellular alterations occur in the mouse sclera with experimental glaucoma and that neural damage can be both augmented and prevented by treatments that affect biomechanical connective tissue responses to IOP in the PPS and astrocytic lamina cribrosa (ALC).[6]

Older age is a significant risk factor for human glaucoma, so defining biomechanical connective tissue behavior in normal and glaucoma eyes according to age is worthy of detailed analysis. Previous studies using ex vivo inflation testing showed that the sclera was stiffer in older human, monkey, dog, and mouse eyes.[7–10] However, most data have been generated from analysis of the sclera in general and not the specific regions of greatest interest: the PPS and LC. We recently developed novel methods for analyzing strains in the PPS and ALC in mice using ex vivo ocular explants.[11] In this report, we measured ALC and PPS biomechanical responses with methods that further improved on imaging, image processing, and strain calculation methodologies. Using multiphoton microscopy and digital volume correlation (DVC), we quantified the deformation of the mouse ALC and PPS in response to acute IOP changes and compared the responses of younger and older mouse eyes.

Methods

Animals

Mice expressing green fluorescent protein under control of the glutamate transporter (GLT1) promoter[12] were acquired from Jeffrey Rothstein (Johns Hopkins School of Medicine, Baltimore, MD, USA).[13] In the primary analysis, 26 younger mice were 2 to 4 months old and 12 older mice were 13 to 15 months old. In studies of the axial length and scleral thickness, we also examined six mice at 2 to 3 months and six mice at 10 to 11 months of age. All animals and experiments were conducted in accordance with guidelines set forth by the ARVO Statement for the Use of Animals in Ophthalmic and Vision Research, using protocols approved and monitored by the Johns Hopkins University School of Medicine Animal Care and Use Committee (Baltimore, MD, USA).

Axial Length and Scleral Thickness Measurements

The axial length and scleral thickness of unfixed enucleated globes were measured in 2- to 3- and 10- to 11-month-old GLT1/GFP mice. For axial length, eyes were measured with a digital caliper (Instant Read Out Digital Caliper; Electron Microscopy Sciences, Hatfield, PA, USA) from the center of the cornea to a position just temporal to the optic nerve insertion. For scleral thickness measurements, the superior scleral quadrant was first cut from the PPS to the limbus. Three strips of sclera, measuring 0.33 mm wide and 2.5 mm long, were thinly sliced with a razor blade and measured at six locations, every 0.5 mm, from the PPS to the limbus with an eyepiece micrometer in a dissecting microscope. For each location, three measurements of scleral thickness were recorded, and the mean of these three measurements were determined for each of the six regions of the three strips for one eye, providing an overall mean for each region. For this report, we present only the thickness data from the PPS region immediately adjacent to the optic nerve head.

Explant Preparation

As previously reported,[11] eyes from 2- to 4-month-old and 13- to 15-month-old GLT1/GFP mice were enucleated, and the optic nerve was removed close to the sclera with a razor blade. The eye was glued, cornea face down, to a plastic fixture. IOP was controlled by a 30-gauge needle placed into the anterior chamber and connected to a manometer filled with 0.1 M Sorenson's PBS. The eye and fixture were placed within a gimbal device permitting rotation about two axes and immersed in PBS at room temperature. The objective lens of the LSM permitted observation of the ALC at a viewing angle perpendicular to its cut surface, that is, parallel to the anterior–posterior axis of the globe, from the exterior side of the eye. The holder rested on the stage of a Zeiss laser-scanning microscope (LSM 710 NLO; Carl-Zeiss, Oberkochen, Germany) with a Chameleon Ultra II laser. The tilt correcting gears on the gimbal were adjusted to align the posterior surface of the ONH perpendicular to the imaging objective.

Imaging

A 20× W Plan Apochromat objective acquired images of the two-photon fluorescence (TPF) signal of the astrocytes of the ALC and the combined second harmonic generation (SHG) and TPF signals of the PPS (SHG-TPF), generated by collagen and elastin, respectively. Imaging of the ALC and PPS required different excitation wavelengths and were imaged sequentially. The ALC was imaged at 895-nm excitation, and data were collected with a 500- to 550-nm band pass filter. For the PPS, both the TPF and SHG were imaged simultaneously using the laser tuned at 780 nm. The TPF signals were captured by a 470- to 550-nm bandwidth filter and the SHG signals by a 390- to 410-nm filter. Baseline IOP was set to 10 mm Hg for 10 minutes and then raised to 30 mm Hg. Images were collected with a resolution of 1024 × 1024 pixels, encompassing a 75-μm z-depth, and were collected with a pixel resolution of 0.415 μm at a pixel dwell time of 0.64 μs to minimize the effects of creep. The x and y direction of images was aligned with the horizontal (nasal–temporal) and vertical (inferior–superior) axes of the ONH, respectively, and the z direction aligned with its anterior–posterior axis.

IOP increase to 30 mm Hg causes an enlargement of the globe with concomitant ONH posterior displacement large enough to move the ALC outside the initial imaging zone. To image the same area after IOP elevation, visible landmarks in the ALC and the PPS were identified prior to elevating IOP. After IOP increase, the starting scan position in the z axis was placed at these landmarks. This z motion was recorded and was later added back to the DVC displacement measurements.

DVC Analysis

For DVC, Z-stacks were reconstructed in a three-dimensional matrix of intensity values in MATLAB (MathWorks, Inc., Natick, MA, USA). The images were postprocessed by a deconvolution function within Huygens Essential (SVI, Hilversum, Netherlands) (Supplemental data: Section S1a). Deconvolution settings were used for Huygens Essential to reduce noise and sharpen structural features within the volumes. For the PPS, the deconvolved SHG and TPF images were combined in ImageJ (National Institutes of Health, Bethesda, MD, USA) into a single SHG-TPF volume, and the contrast of the combined volume was enhanced prior to DVC using a contrast-limited adaptive piecewise histogram equalization algorithm (Supplemental Data: Section S1b).

The fast-iterative DVC algorithm developed by Bar-Kochba et al.[14] was used to obtain the three-dimensional displacement field from the TPF image of the ALC and SHG-TPF image of the PPS for inflation from 10 to 30 mm Hg. This DVC algorithm maximizes the cross-correlation of the image intensity of subvolumes in the reference images at 10 mm Hg and deformed images at 30 mm Hg to determine the displacements

Investigative Ophthalmology & Visual Science

Table 1. Symbol Nomenclature for the Measured Strains

Symbol	Strain Name	Strain Measurement
E_{max}	Maximum principal strain	Maximum tensile strain along its maximum direction
S_{max}	Maximum shear strain	Maximum shear strain along its maximum directions
E_{xx}	NT strain	Elongational strain in the nasal-temporal direction
E_{yy}	IS strain	Elongational strain in the inferior-superior direction
E_{xy}	Shear strain	Angular distortion between the nasal-temporal and inferior-superior directions
E_{rr}	Radial strain	Elongational strain along the radial direction
E_{tt}	Circumferential strain	Elongational strain along the circumferential (hoop) direction
E_{rt}	Radial–circumferential shear strain	Angular distortion between the circumferential and radial directions

with IOP increase.[14] The algorithm iteratively refines the subvolume size and calculation spacing to improve the correlation in a four-step process starting with a subset size of $128 \times 128 \times 64$ pixels and calculation spacing of $32 \times 32 \times 16$ pixels, and ending with a final subset size of $32 \times 32 \times 16$ and spacing of $4 \times 4 \times 1$ pixels. The cross-correlation coefficient provided by the fast-iterative DVC algorithm was exported for analysis along with the components of the calculated displacement field at each point. The displacements were converted from pixels to micrometers based on the known voxel size of $0.415 \times 0.415 \times 1$ μm/pixel in x, y, and z prior to strain calculation.

Postprocessing DVC Displacements and Strain Calculation

ALC and PPS Baseline Error. Prior to calculating strains, regions of high correlation error in the DVC displacement were removed. We then estimated the DVC baseline positional error, displacement correlation error, and strain calculation error as shown in Nguyen et al.[11] and Supplemental Data: Section S2. We correlated duplicate Z-stacks acquired for each volume at the 10 mm Hg baseline. Because the volumes were acquired under nominally identical conditions, the displacements and strains obtained from DVC estimate the errors associated with image quality and tissue creep during image acquisition. Next, we estimated the DVC displacement correlation and strain error under a uniform strain by numerically applying displacements and strains to one of the duplicate Z-stacks taken at 10 mm Hg (Supplemental Data: Section S2). The resulting DVC estimated error included the effect of feature distortion by deformation, as well as the effects of image quality and tissue creep. These error analyses were performed separately for the PPS and ALC images.

Within the mouse PPS and ALC, there were regions of low contrast that did not correlate and were excluded prior to strain calculation. For instance, the PPS has a zone of blood vessels that enter the inferior ONH forming a V-shaped notch, which does not have enough contrast to obtain a displacement correlation. In addition, areas within the PPS of some eyes were outside of the imaging range and remained dark. Within the ALC, the signal was sometimes indistinct in the peripheral ALC. Due to the higher measured strain errors in the peripheral ALC, we chose to investigate the central two-thirds and central one-half of the ALC because it was more accurate than the peripheral strains. We therefore calculated both the overall strains of the ALC and the strains in the central ALC alone.

ALC Deformation. Within the ALC, poorly correlating regions were excluded by removing DVC results with a cross-correlation coefficient of ≤ 0.001 and regions that had a DVC displacement error of ≥ 1 μm (2.5 pixels). The remaining displacements were smoothed prior to strain calculation using a three-dimensional Gaussian filter with a width of $21 \times 21 \times 21$ μm and an SD of $5 \times 5 \times 5$ μm.[2]

The Green-Lagrange strains for the ALC were evaluated from the x, y, and z displacement fields by fitting a fourth-order polynomial function to each displacement component in the x and y directions and a linear function in z, evaluating the displacement gradients, and calculating the strain tensor (Supplemental Data: Section S3).

PPS Deformation. Likewise, within the PPS, poorly correlating regions were excluded from analysis by removing DVC calculations with a cross-correlation coefficient threshold of 0.015 or less and areas within the volumes that had a DVC displacement error of 2 μm (5.0 pixels) or more. The displacement field in the PPS was noisier than in the ALC, and a displacement filter was used to remove displacement outliers that deviated by more than 8 μm from the average within an 18- × 18-μm region. We were only able to image features within the PPS up to a depth of 10 μm. Moreover, the subsurface features appeared to be shadowed by features on the surface of the PPS. Thus, we were not able to produce accurate calculations of anterior–posterior PPS strain (z axis). To calculate the strain in x and y, the displacements were projected to a plane. A two-dimensional version of the Gaussian smoothing filter with a width of 25×25 μm and an SD of 10×10 μm was applied to smooth the displacements prior to strain calculation. Displacement calculations within 10 μm of the image edges were removed as these areas tended to have larger errors.

Due to the asymmetric shape of the correlating regions within the PPS compared with the ALC, a more localized strain calculation method was required. A plane was fit to the displacement components in a 35- × 35-point (58- × 58-μm) region around each displacement calculation to calculate the displacement gradients in x and y (Supplemental Data: Section S3). The Lagrangian strains E_{XX} (nasal–temporal strain), E_{YY} (inferior–superior strain), and E_{XY} (shear strain) were obtained at each point from the displacement gradients in x and y (Supplemental Data: Section S3). Strains were not calculated if more than 50% of the surrounding points in the 58- × 58-μm area did not correlate.

The in-plane components of the Lagrangian strain tensor (E_{XX}, E_{YY}, and E_{XY}) were used to calculate the maximum principal strain, E_{max}, and the maximum shear strain, S_{max}, in the plane as shown in Supplemental Data: Section S3. The cylindrical components of the strain tensors, E_{rr} (radial strain), E_{tt} (circumferential strain), and E_{rt} (radial–circumferential shear strain) were calculated as shown in Supplemental Data: Section S3. The physical significance of the strain measures are described in Table 1.

Perimeter Tracing and Regional Strains

As previously reported,[11] the change in the length of the ALC perimeter (the circumference of the ALC) was measured by delineating it on maximum intensity projections of the TPF images at both 10 and 30 mm Hg. From the ellipse that was

Investigative Ophthalmology & Visual Science

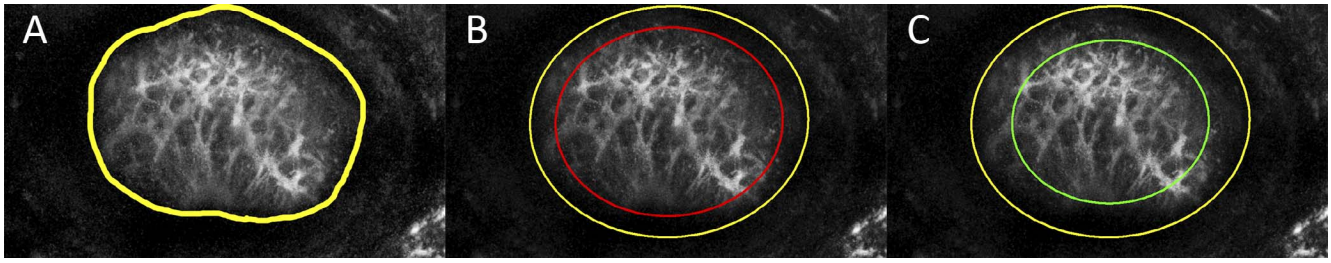

Figure 1. Delineation of lamina cribrosa zones. (**A**) The outer perimeter of the lamina cribrosa was identified as the most peripheral zone with fluorescent astrocyte processes (*yellow line*). (**B**) This perimeter was fit to an ellipse (*yellow*) and used for overall (global) lamina strain estimations. In addition, ALC strains were estimated in two central regions, one occupying the central two-thirds of the lamina area (outlined in *red line* in **B**) and one occupying one-half of the lamina area (outlined in *green line* in **C**).

fitted to the perimeter of the ALC, the diameter in the nasal–temporal (major) axis and its diameter in the inferior–superior (minor) axis were calculated. The globe and nerve orientation were preserved carefully during mounting of each eye to identify the superior pole. The percent perimeter change was calculated by taking the perimeter at 30 mm Hg minus that at 10 mm Hg, divided by the perimeter at 10 mm Hg. This marked perimeter was also used to delimit the zone within which regional strains in the central ALC were calculated. Two central ALC zones were constructed, one occupying two-thirds of the overall ALC area within the perimeter and one comprising one-half of the ALC area (Fig. 1). To do this, an ellipse was fit to perimeter tracings at 10 mm Hg, and two smaller, concentric elliptical areas, one with two-thirds and one with one-half of the area of the outer ellipse, were marked. The strains within these two zones were denoted central strains.

The PPS of the mouse has a <50 μm wide zone of circumferentially arranged collagen and elastin fibers at its junction with the astrocyte end feet. Beyond this zone, which has an outer region containing many fibroblasts, the broader zone of PPS extends away from the ONH with a rapidly decreasing degree of collagen and elastin anisotropy, with alternating layers of fiber lamellae containing fibers in each layer that are parallel to each other. The thin zone of circumferential fibers is too small to use DVC techniques for strain estimation. For this reason, we provide the perimeter data, which directly show enlargement of this zone with IOP increase. Our PPS strain estimates are made from the sclera just outside this astrocyte–sclera junction, extending at the edge of LSM images for as much as 200 μm (Fig. 2).

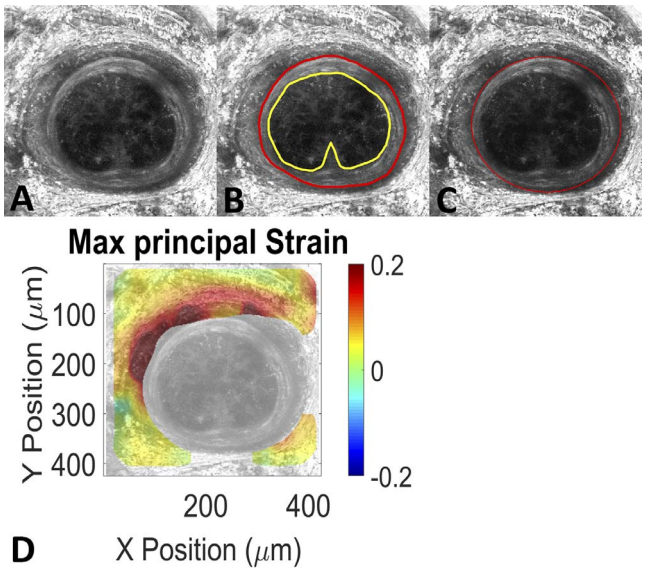

Figure 2. Delineation of peripapillary sclera. (**A**) Two-dimensional, maximum intensity projection of the PPS; (**B**) PPS delineation was performed by marking the outer margin of the contact zone between astrocytes and sclera (*red circle*). Between this and the termination of astrocyte endfeet (*yellow line*, as in Fig. 1) is the zone of circumferentially arranged connective tissue fibers. The displacement related to this area between the *yellow* and *red* zones was estimated by the ALC perimeter measurements. (**C**) The PPS strains estimated by DVC included the zone outside an ellipse fitted to the marked *red line* in **B**. (**D**) An example of a maximum PPS strain plot calculated in this way with the two-dimensional maximum intensity projection overlayed.

Statistical Testing

The axial length and scleral thickness measurements, the ALC and PPS strains, and the change in perimeter measurements were analyzed using generalized estimating equation (GEE) linear models that took into account the correlation in outcome between two eyes of a single mouse for mice where both eyes were tested. The models used the normal probability distribution and the identity link function. For each strain analyzed, a GEE model was used to test whether the outcome was significantly greater than zero for younger or older mice and whether the outcome was significantly different between the two age groups. A second model was used to test whether the outcome differed significantly for male and female mice. Additional models tested the difference between outcomes in the nasal–temporal and inferior–superior directions for all mice and by age group. A result was considered statistically significant if the P value after accounting for bilateral data was <0.05. The Bonferroni method was used to adjust for multiple comparisons. All analyses were performed using SAS 9.2 (SAS Institute, Cary, NC, USA).

Results

Axial Length and Scleral Thickness Measurements With Age in Mice

We measured axial lengths and scleral thickness in six GLT1/GFP mice at 2 to 3 months and six mice at 10 to 11 months of age. At 2 to 3 months, the mean axial length and mean PPS thickness in fresh, unfixed eyes were 3.16 ± 0.04 mm and 37.17 ± 3.21 μm, respectively ($n = 12$ eyes of six mice; Table 2). At age 10 to 11 months, the mean axial length of unfixed eyes and mean PPS thickness was 3.59 ± 0.02 mm and 31.27 ± 1.70 μm, respectively ($n = 12$ eyes of six mice). The 10- to 11-month-old mice had significantly longer axial lengths and significantly thinner PPS than the 2- to 3-month-old mice (Table 2). Data from 17- to 18-month-old mice of this background are even longer and have thinner sclera than the 2- to 3-month-old mice (data not shown), thus confirming that the older animals

Investigative Ophthalmology & Visual Science

Table 2. Axial Length and PPS Thickness

Outcome	Age, mo	Mean (95% CI)	*P* for Effect of Age	Adjusted *P**
Axial length, mm	2–3	3.2 (3.1, 3.2)	**<0.0001**	**<0.0003**
	10–11	3.6 (3.6, 3.6)		
PPS thickness, μm	2–3	37.2 (35.1, 39.3)	**<0.0001**	**<0.0003**
	10–11	31.3 (30.7, 31.9)		

Bold values represent statistical significance.
* Bonferroni adjustment for multiple comparisons. CI, confidence interval.

whose strain estimates are provided here have longer eyes and thinner PPS than the younger mice. Of the 2- to 3-month-old mice, eight eyes were from four female mice, and four eyes from two male mice. Of the 10- to 11-month-old mice, six eyes were from three female mice and six eyes from three male mice. There was no difference by sex (Supplemental Data: Section S4).

ALC Strain

The normal and shear strain components in the x–y plane were calculated from displacement data for a total of 54 eyes of 38 mice (Fig. 3; x denotes the nasal–temporal and y denotes the inferior–superior directions). Data for all strain measures (Table 1) are given for ALC and PPS in Supplemental Data: Sections S5 and S7. Here, we present results for the strain components in the x (nasal–temporal) and y (inferior–superior) directions for the ALC and for the radial and circumferential directions in the PPS. This is due to the fact that the nasal–temporal–inferior–superior strains are more physiologic descriptors for the behavior of the ALC, whereas the radial–circumferential strains are more physiologic descriptions for the PPS. In addition, results are presented for the maximum principal strain and the maximum shear strains, which are the magnitude of the tensile and shear strains in the directions in the x–y plane along which they are maximum. We do not present the strain components in the anterior–posterior (z) directions in the ALC because they were associated with large strain errors in the DVC error analysis.

Globally averaged strains were significantly greater than zero for all strains in younger mice and for all strains except inferior–superior strain in older mice (Table 3: in this table and those following, the first column of *P* values indicates whether the individual value for an age group differed from zero, whereas the *P* value column "*P* age" gives the significance of any of the differences between the two age groups in that parameter). Inferior–superior strain was 2.4% in younger mice,

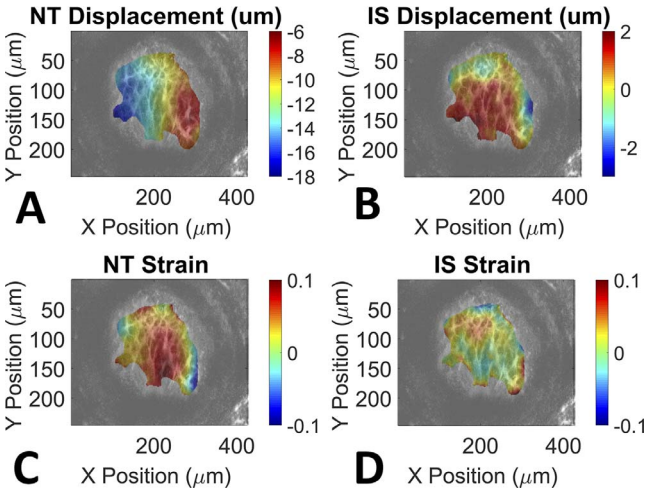

Figure 3. Example of DVC-calculated displacements and strains. Typical displacement (**A**, **B**) and strain (**C**, **D**) estimates from DVC for the mouse ALC. In each image, superior is at *top*, nasal at *right*. NT, nasal–temporal displacement field and strain; IS, inferior–superior displacement field and strain. *Color bar* units for the displacement plots are micrometers, and strain is unitless.

but in older mice, strain in this direction was negligible (age difference: $P = 0.002$). All other strain measures were also smaller in older than younger animals, but the comparisons were not statistically significant because of the large variations.

The strain data for the central two-thirds of the ALC were similar to the overall, global ALC strains (Table 4). All strains were significantly greater than zero regardless of age, except for inferior–superior strain in older mice, which was significantly less than that of younger mice ($P = 0.01$).

Strain data are unitless (micrometer/micrometer). *P* values for each strain and for the difference by age are from GEE models.

We compared male with female mouse ALC strains in models for both global and central two-thirds ALC. Of the younger mice, 14 eyes were from 10 female mice and 22 eyes were from 16 male mice. Of the older mice, 6 eyes were from six female mice and 10 eyes were from six male mice. There were no significant differences in any of the five strains included in Tables 3 and 4 by sex (*P* values for difference by sex for global ALC strains varied from 0.58 to 0.95).

ALC Area, Perimeter Length, and Diameter

Measures of ALC area, perimeter length, and diameters were used to estimate displacement of the thin region of PPS that

Table 3. ALC Global Strains

Global ALC Strains	Age	Mean (95% CI)	*P* Difference From 0	*P* Age
NT strain	Younger	0.043 (0.032, 0.054)	**<0.0001**	0.85
	Older	0.040 (0.013, 0.067)	**0.004**	
IS strain	Younger	0.024 (0.011, 0.037)	**0.0004**	**0.002**
	Older	0.001 (−0.005, 0.007)	0.65	
Shear strain	Younger	0.044 (0.032, 0.057)	**<0.0001**	0.08
	Older	0.030 (0.019, 0.040)	**<0.0001**	
Max principal strain	Younger	0.116 (0.082, 0.150)	**<0.0001**	0.13
	Older	0.077 (0.041, 0.114)	**<0.0001**	
Max shear strain	Younger	0.083 (0.060, 0.107)	**<0.0001**	0.14
	Older	0.058 (0.033, 0.082)	**<0.0001**	

Strain data are unitless (micrometer/micrometer). *P* values for each strain and for the difference by age are from GEE models. Bold values represent statistical significance. IS, inferior–superior; Max, maximum; NT, nasal–temporal.

Table 4. Central Two-Thirds ALC Strains

Central 2/3 ALC Strains	Age	Mean (95% CI)	*P* Difference From 0	*P* Age
NT strain	Younger	0.046 (0.035, 0.057)	**<0.0001**	0.75
	Older	0.042 (0.015, 0.068)	**0.002**	
IS strain	Younger	0.019 (0.006, 0.033)	**0.004**	**0.01**
	Older	−0.0006 (−0.008, 0.006)	0.88	
Shear strain	Younger	0.042 (0.030, 0.055)	**<0.0001**	0.10
	Older	0.028 (0.017, 0.039)	**<0.0001**	
Max principal strain	Younger	0.112 (0.079, 0.146)	**<0.0001**	0.13
	Older	0.075 (0.039, 0.110)	**<0.0001**	
Max shear strain	Younger	0.079 (0.056, 0.103)	**<0.0001**	0.16
	Older	0.055 (0.031, 0.080)	**<0.0001**	

Bold values represent statistical significance.

immediately contacts the astrocytes of the ALC, which is too thin for DVC analysis. In baseline images at 10 mm Hg, the area and inferior–superior diameter of younger mice were significantly smaller than those in older mice (Table 5). There were no significant differences in perimeter and nasal–temporal diameter by age.

We assessed the change with inflation of these ALC parameters (Table 6). The mean ALC area, perimeter length, and nasal–temporal diameter increased with inflation for both groups of mice, but the increase was statistically greater in younger mice. Although young mice had a significant increase in ALC inferior–superior diameter, older mice did not, but there was no significant difference in this parameter by age.

PPS Strains

PPS strain data were obtained in 35 eyes from 14 younger and 13 older mice that satisfied our criteria for adequate DVC correlation (Fig. 4; Table 7). The radial and circumferential strains, as well as the radial–circumferential shear strains, exhibited large variations within each specimen; however, only the average radial and circumferential strains were statistically greater than zero ($P \leq 0.001$), whereas the average shear strain was not statistically different than zero. The average radial strains were two times greater than the circumferential strains. Circumferential strains were significant for both age groups ($P = 0.001$ for younger and $P < 0.0001$ for older). The average maximum principal strain and radial strain were larger in older than younger eyes, but these differences were not significant. Likewise, the maximum shear strain was larger in older eyes and this was the only significant difference by age.

Some specimens did not have the entire circumference of the PPS available for DVC correlation, or they did not satisfy our criteria for accurate DVC correlation in all areas of the sclera. We therefore selected eight young and eight old eyes that had the most complete PPS areas of DVC correlation for PPS strain calculation (Table 8). As with the overall group of eyes, all but the radial–circumferential shear strain were significantly different from zero in both age groups. In this selected subgroup, the maximum principal, maximum shear, and radial strains were all significantly larger in older than younger animals.

We constructed statistical models for PPS strains that compared male with female mice. As with the ALC strains, there were no significant differences by sex (*P* varied from 0.30 to 0.74 for the five strains shown in Table 7, column 1).

Table 5. Baseline ALC Perimeter Data

Baseline Perimeter Measurements	Age	Mean (95% CI)	*P* Age
Area	Younger	47,129 (45,173, 49,085)	**0.05**
	Older	50,873 (47,686, 54,059)	
Perimeter	Younger	800.3 (783.0, 817.6)	0.16
	Older	824.5 (795.8, 853.3)	
NT diameter	Younger	286.3 (279.1, 293.5)	0.67
	Older	289.5 (277.3, 301.7)	
IS diameter	Younger	208.8 (203.7, 214.0)	**0.0004**
	Older	223.4 (217.2, 229.6)	

Area units are μm^2. Perimeter, NT diameter, and IS diameter in μm. GEE models adjusting for bilateral eye data. Bold values represent statistical significance.

Discussion

Methods to study the behavior of ONH tissues are highly relevant to our understanding of the mechanisms of axonal damage in glaucoma. Mouse models of normal aging and experimental glaucoma have both advantages and disadvantages in elucidating glaucoma mechanisms. Mouse longevity is short relative to humans, making study of older animals feasible in shorter time frames, but mouse models lack the long-term, environmental, and disease-related effects in the aging human eye. In this study, we developed improvements in our methods to measure the biomechanical response to acute IOP elevation of the ALC, which is the immediate contact zone between ALC and PPS, and the wider zone of PPS in the mouse eye. Our ultimate aim is to construct models of the behavior of the ALC and PPS together as a unitary structure.

The present data show that the ALC and PPS in mice undergo strains with acute IOP inflation that are consistent with strain magnitudes measured in prior work for the mouse posterior sclera[10,11] and for the human LC[2] and posterior sclera.[7] Our methods have been refined to take into account the specific anatomy of the mouse ONH area. Subanalysis of the central ALC and consideration of PPS data after removal of outlying values did not change the primary findings. There were no differences between male and female mice in any measure. In mouse ALC, there was greater strain in the nasal–temporal direction than in the inferior–superior direction. This was true in both younger and older mice ALC and confirms an initial study by less extensive methods in our prior study.[11] There was also greater increase in ALC diameter in the nasal–temporal axis compared with inferior–superiorly with acute IOP elevation. This is compatible with the horizontally oval shape of the mouse ONH and may result in part from the presence of blood vessels passing through the inferior ONH to the retina. There is considerable evidence that the lower density of connective tissue[15] and regionally greater strains[2] in the upper and lower quadrants of the human LC contribute to

Investigative Ophthalmology & Visual Science

Table 6. ALC Perimeter Percent Change From Baseline

ALC Perimeter Data	Age	Mean (95% CI)	*P* Difference From 0	*P* Age
Area change	Younger	5.76% (4.82, 6.69)	**<0.0001**	**0.004**
	Older	3.57% (2.39, 4.75)	**<0.0001**	
Perimeter elongation	Younger	3.35% (2.90, 3.80)	**<0.0001**	**<0.0001**
	Older	1.83% (1.27, 2.39)	**<0.0001**	
NT diameter change	Younger	4.75% (3.90, 5.60)	**<0.0001**	**0.01**
	Older	3.25% (2.50, 4.01)	**<0.0001**	
IS diameter change	Younger	1.05% (0.18, 1.92)	**0.02**	0.35
	Older	0.37% (−0.77, 1.51)	0.52	

Change is shown as percent compared with baseline. GEE models adjusting for bilateral eye data. Bold values represent statistical significance.

Table 7. PPS Strains

PPS Strains	Age	Mean (95% CI)	*P* Difference From 0	*P* Age
Max principal strain	Younger	0.041 (0.030, 0.052)	**<0.0001**	0.08
	Older	0.058 (0.043, 0.074)	**<0.0001**	
Max shear strain	Younger	0.024 (0.019, 0.030)	**<0.0001**	**0.002**
	Older	0.040 (0.032, 0.048)	**<0.0001**	
Radial strain	Younger	0.022 (0.014, 0.031)	**<0.0001**	0.24
	Older	0.032 (0.019, 0.044)	**<0.0001**	
Circumferential strain	Younger	0.007 (0.003, 0.011)	**0.001**	0.40
	Older	0.009 (0.007, 0.010)	**<0.0001**	
Radial–circumferential shear strain	Younger	−0.0004 (−0.0025, 0.0017)	0.69	0.90
	Older	−0.0001 (−0.0052, 0.0051)	0.98	

Strain data are unitless (micrometer/micrometer). *P* values for each strain and for the difference by age are from GEE models adjusting for bilateral eye data. Bold values represent statistical significance.

Table 8. PPS Strains in Eyes With Highest Area of Correlation

PPS Strains	Age	Mean (95% CI)	*P* Difference From 0	*P* Age
Max principal strain	Younger	0.034 (0.029, 0.040)	**<0.0001**	**0.01**
	Older	0.073 (0.046, 0.101)	**<0.0001**	
Max shear strain	Younger	0.022 (0.019, 0.026)	**<0.0001**	**0.002**
	Older	0.046 (0.032, 0.060)	**<0.0001**	
Radial strain	Younger	0.015 (0.008, 0.022)	**<0.0001**	**0.01**
	Older	0.046 (0.023, 0.070)	**0.0001**	
Circumferential strain	Younger	0.010 (0.007, 0.013)	**<0.0001**	0.70
	Older	0.008 (0.002, 0.015)	**0.01**	
Radial–circumferential shear strain	Younger	0.0005 (−0.0017, 0.0028)	0.64	0.35
	Older	−0.0036 (−0.0120, 0.0047)	0.39	

Strain data are unitless (micrometer/micrometer). *P* values for each strain and for the difference by age are from GEE models adjusting for bilateral eye data. Bold values represent statistical significance.

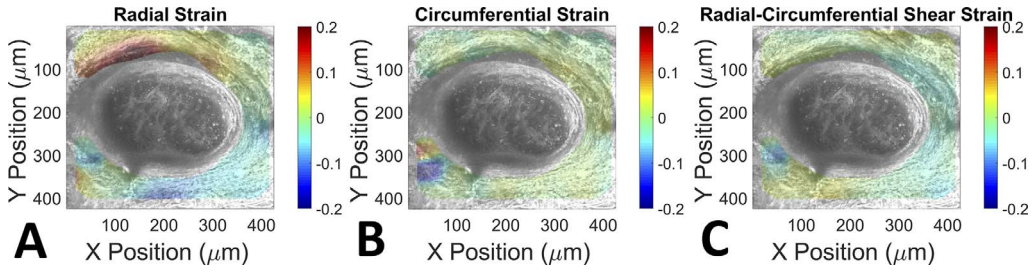

Figure 4. PPS strain maps. Typical PPS strain maps for radial strain (**A**), circumferential strain (**B**), and radial–circumferential shear strain (**C**). The colorbar for strain plots are unitless.

regionally greater loss of axons from the upper and lower poles of the ONH and explain the typical pattern of visual field loss. There is regionally greater loss of axons in the superior and temporal optic nerve in moderately damaged eyes of mice with chronic experimental glaucoma.[16] Our previous studies of this regional loss were carried out in CD1 albino and C57BL/6 pigmented mice. Further study of GLT1/GFP mice is ongoing to compare the present inflation data to regional loss in this mouse type. GLT1/GFP mice are intermediate in the susceptibility to overall ganglion cell loss, falling between those of the more susceptible CD1 mice and the relatively resistant C57BL/6 mice (data not shown). Whether there is regional ganglion cell loss in GLT1/GFP mice is the subject of ongoing study. GLT1/GFP mice are agouti, that is, partially pigmented, compared with albino CD1 and pigmented C57BL/6 mice. The details of regional loss may not be similar between human LC and mouse ALC, because there is no connective tissue in the mouse ALC and the shape of the ALC and other factors are quite different.

ALC strains were greater in younger mouse eyes than in older eyes in the inferior–superior direction, but not in the nasal–temporal direction, both in global calculations and when only the central ALC was included. Similarly, the younger eyes had greater increases than older mice in the two-dimensional–projected ALC area, ALC perimeter, and nasal–temporal ALC diameter, which measure displacement in the immediate contact zone of PPS to ALC. These changes in the ALC perimeter and diameter reflect the effects of scleral canal expansion with IOP, whereas ALC strains include the response of astrocytes to scleral canal expansion and posterior deflection of the ALC. The findings are consistent with ex vivo measurements of increased stiffness of collagenous tissues with age and specifically of decreased strains in LC[2] and PPS[17] of human eyes with age. However, the behavior of the mouse ALC as measured here results both from the response of astrocytes and from their attachment to the adjacent PPS. The older mice had significantly smaller enlargement of the immediate contact zone between PPS and astrocytes, indicating a stiffer behavior of the zone of circumferentially arranged collagen and elastin fibers.

Within the PPS just outside the immediate contact zone, the measured radial and circumferential strains in mice were also significantly greater than zero, which is consistent with measurable ALC strains and ALC area enlargement. The average radial and circumferential strains were 2% to 3% and less than 1%, respectively. Although it might be expected that PPS strains would be smaller in older than in younger mice, they were, in fact, not significantly different from younger mice when all eyes were included in most measures. In data from all mice, maximum shear strain was actually greater in older mice. Furthermore, in subanalysis of eyes with the most complete data, older mice had larger maximum principal strain, maximum shear strain, and radial strain in the PPS. This finding seems to differ from our previous scleral inflation study in mice[8] that suggested lower strain in older mouse eyes. However, the methods and location of strain measurement, as well as type of mouse, differed between these studies. Our earlier report estimated scleral strain using two-dimensional digital image correlation that could only measure displacement of the overall profile of the posterior scleral edge under a dissecting microscope. The present method is based on DVC and laser scanning microscope images. In our previous study, we could not determine strain in the PPS close to the ONH, which has a regionally unique fiber arrangement that is quite different from the alternating directions of fiber lamellae in the overall posterior sclera. The average circumferential strain in the PPS was significantly smaller than the 3% value that was measured further from the ONH in prior inflation studies using two-dimensional imaging.

The PPS strains measured here are influenced by differences between younger and older eyes in axial globe length and scleral thickness. The eyes of older GLT1/GFP mice were significantly longer and their PPS was thinner than for younger mice. The ratio of the axial length to the thickness of the PPS, an important factor determining the IOP-induced stresses in the sclera, was 35% larger in older eyes. Other factors that may influence the PPS strains include the baseline size of the ONH, and the inner border of the PPS region was larger at baseline in the older animals. Strains may also be influenced by the degree of fiber anisotropy, a feature that we are presently studying in GLT1/GFP mice at various ages. Experimental glaucoma reduces the circumferential orientation of fibers in the mouse PPS.[18,19] Computational modeling is needed to analyze the inflation data and separate the effects of geometry differences from those of age-related changes in the stiffness and anisotropy of the PPS and ALC.

We purposefully used the terms younger and older in referring to the two groups of mice undergoing inflation testing here. From a practical matter, maintaining mice for testing at even older ages than those studied is difficult, as they neither survive nor tolerate surgical manipulations well. It is worth considering that 2-month-old mice are mature enough for reproduction but may correspond more to juvenile humans. It could therefore be argued that our comparison is similar to contrasting teenage to middle-aged human eyes. In monkeys, Girard et al. reported that PPS was thicker in adult than juvenile monkeys and then thinner again in very aged animals.[8] Initial studies of the biomechanical behavior of human glaucoma eyes only used surface labeling of the posterior sclera.[20] Coudrillier et al. reported that human PPS was thinner in very elderly (80 to 90 years old) compared with middle-aged adults (40 to 50 years old), but few human juvenile eyes have been so studied.[17] These differences must be taken into account in comparing rodent and primate sclera.

The effect of age on ganglion cell loss in chronic mouse glaucoma models has been shown to differ by mouse type. C57BL/6 mice were more susceptible to axon loss in older than in younger animals, whereas older CD1 mice were less likely to lose ganglion cells than younger CD1 mice.[21–23] CD1 mice have significantly larger axial length than C57BL/6 mice, and their scleral thicknesses differ modestly. Furthermore, in each mouse type axial length increases with age. We are now studying the comparative ALC and PPS strains in these types of mice to determine if they relate to relative glaucoma susceptibility.

More detailed modeling of the ONH response to IOP should take into account the effect of nonfiber elements in PPS. In human eyes, the most significant difference in scleral components with older age was a greater effect on the nonfibrous matrix component.[24] This important contribution to the biomechanics of the human sclera by the nonfibrous extracellular matrix was demonstrated when glycosaminoglycans were removed by enzymatic treatment ex vivo, leading to a stiffer inflation response.[25,26]

Recent studies using optical coherence tomography in living glaucoma patient eyes indicate that the amount and direction of LC movement with acute IOP change depend on the severity of glaucoma injury.[3] This is likely due to remodeling of the LC and PPS and provides direct evidence that the state of both LC and PPS are dynamically changing and interdependent. In both CD1 and C57BL/6 mice, exposure to chronic IOP elevation results in axial globe elongation and stiffer pressure–strain responses for both the effective circumferential and meridional strains of the equatorial sclera.[27] More importantly, experimental glaucoma leads to cell division and

Investigative Ophthalmology & Visual Science

increased metabolism of PPS fibroblasts.[28] In human glaucoma, it is well established that the incidence, prevalence, and progressive worsening of disease increase with age.[29] It is therefore difficult to separate the effect of age and the effect of disease duration on the mechanical response of the eye and the presence and severity of glaucoma damage. With a chronic disease, the dynamically changing effect of disease and increasing age are simultaneous.

It is likely that the substantial influence of PPS and ALC structure and remodeling can be harnessed to develop treatments that benefit the glaucoma patient. Genetic modification of collagens is protective in a mouse model.[23] Increased cross-linking of scleral collagens with glyceraldehyde treatment increased the loss of ganglion cells in experimental mouse glaucoma.[30] By contrast, alteration of the connective tissue remodeling in the mouse sclera in experimental glaucoma by oral losartan treatment reduced axonal transport disruption and protected against ultimate ganglion cell death.[6] It is feasible that local treatments using sustained delivery of agents to the sclera can be developed as neuroprotective strategies in glaucoma.[31]

Our research had some limitations. To avoid the effects of creep, we used a short pixel dwell time to image the ALC and PPS. As a result, the TPF and SHG images had more noise than if longer dwell times were possible. Further, some regions of the images exhibited poor contrast, affecting the accuracy of DVC displacement calculations. The TPF and SHG images also had relatively low resolution in the anterior–posterior direction, resulting in higher than ideal error in out-of-plane strains. The present analysis depends on an ex vivo explant model, and, although the eyes are enucleated and studied less than 2 hours postmortem, the stress–strain relationship may be different from that in vivo. The behavior of the ALC and PPS is likely to be altered through remodeling of the cells and tissues with chronic IOP elevation, and study of the effect of these phenomena is ongoing.

In summary, we measured the stress–strain response of the mouse eye at the ONH and found values for ALC strain and enlargement of the ALC circumference that are greater in the nasal–temporal direction. PPS strains were significant in the radial and circumferential directions. Older eyes had less ALC strain and ALC enlargement, whereas their PPS strain was greater than that in younger sclera, although these strains are affected by the larger axial lengths and thinner sclera of older eyes. There were no differences between male and female mice.

Acknowledgments

Supported by Public Health Service (PHS) Research Grants EY 02120 and EY 01765 (HG, and Wilmer Institute Core Grant), EY021500 (CN), National Science Foundation CAREER Award 1253453 (CN), and unrestricted support from Saranne and Livingston Kosberg, William T. Forrester, and Troy Williams. The funders had no role in study design, data collection and analysis, decision to publish, or preparation of the manuscript.

Disclosure: **C. Nguyen**, None; **D. Midgett**, None; **E. Kimball**, None; **J. Jefferys**, None; **T.D. Nguyen**, None; **J. Schaub**, None; **M. Pease**, None; **H. Quigley**, None

References

1. Quigley HA, Broman A. The number of persons with glaucoma worldwide in 2010 and 2020. *Br J Ophthalmol*. 2006;90:151–156.
2. Midgett DE, Pease ME, Jefferys JL, et al. The pressure-induced deformation response of the human lamina cribrosa: analysis of regional variations. *Acta Biomater*. 2017;53:123–139.
3. Quigley H, Arora K, Idrees S, et al. Biomechanical responses of lamina cribrosa to intraocular pressure change assessed by optical coherence tomography in glaucoma eyes. *Invest Ophthalmol Vis Sci*. 2017;58:2566–2577.
4. Sun D, Lye-Barthel M, Masland RH, Jakobs TC. The morphology and spatial arrangement of astrocytes in the optic nerve head of the mouse. *J Comp Neurol*. 2009;516:1–19.
5. Anderson DR. Ultrastructure of human and monkey lamina cribrosa and optic nerve head. *Arch Ophthalmol*. 1969;82:800–814.
6. Quigley HA, Pitha IF, Welsbie DS, et al. Losartan treatment protects retinal ganglion cells and alters scleral remodeling in experimental glaucoma. *PLoS One*. 2015;10:e0141137.
7. Coudrillier B, Pijanka J, Jefferys J, et al. Effects of age and diabetes on scleral stiffness. *J Biomech Eng*. 2015;137:071007.
8. Girard MJA, Suh JKF, Bottlang M, Burgoyne CF, Downs JC. Scleral biomechanics in the aging monkey eye. *Invest Ophthalmol Vis Sci*. 2009;50:5226–5237.
9. Palko JR, Morris HJ, Pan X, et al. Influence of age on ocular biomechanical properties in a canine glaucoma model with *ADAMTS10* mutation. *PLoS One*. 2016;11:e0156466.
10. Myers KM, Cone FE, Quigley HA, Gelman S, Pease ME, Nguyen TD. The in vitro inflation response of mouse sclera. *Exp Eye Res*. 2010;91:866–875.
11. Nguyen C, Midgett D, Kimball EC, et al. Measuring deformation in the mouse optic nerve head and peripapillary sclera. *Invest Ophthalmol Vis Sci*. 2017;58:721–733.
12. Benediktsson AM, Marrs GS, Tu JC, et al. Neuronal activity regulates glutamate transporter dynamics in developing astrocytes. *Glia*. 2012;60:175–188.
13. Regan MR, Huang YH, Kim YS, et al. Variations in promo'ter activity reveal a differential expression and physiology of glutamate transporters by glia in the developing and mature CNS. *J Neurosci*. 2007;27:6607–6619.
14. Bar-Kochba E, Toyjanova J, Andrews E, Kim K, Franck C. A fast iterative digital volume correlation algorithm for large deformations. *Exp Mech*. 2015;55:261–274.
15. Quigley HA, Addicks EM. Regional differences in the structure of the lamina cribrosa and their relation to glaucomatous optic nerve damage. *Arch Ophthalmol*. 1981;99:137–143.
16. Schaub JA, Kimball EC, Steinhart MR, et al. Regional retinal ganglion cell axon loss in a murine glaucoma model. *Invest Ophthalmol Vis Sci*. 2017;58:2765–2773.
17. Coudrillier B, Tian J, Alexander S, Myers KM, Quigley HA, Nguyen TD. Biomechanics of the human posterior sclera: age- and glaucoma-related changes measured using inflation testing. *Invest Ophthalmol Vis Sci*. 2012;53:1714–1728.
18. Pijanka JK, Kimball EC, Pease ME, et al. Changes in scleral collagen organization in murine chronic experimental glaucoma. *Invest Ophthalmol Vis Sci*. 2014;55:6554–6564.
19. Pijanka JK, Coudrillier B, Ziegler K, et al. Quantitative mapping of collagen fiber orientation in non-glaucoma and glaucoma posterior human sclerae. *Invest Ophthalmol Vis Sci*. 2012;53:5258–5270.
20. Coudrillier B, Pijanka JK, Jefferys JL, et al. Glaucoma-related changes in the mechanical properties and collagen microarchitecture of the human sclera. *PLoS One*. 2015;10:e0131396.
21. Cone FE, Steinhart MR, Oglesby EN, Kalesnykas G, Pease ME, Quigley HA. The effects of anesthesia, mouse strain and age on intraocular pressure and an improved murine model of experimental glaucoma. *Exp Eye Res*. 2012;99:27–35.
22. Cone FE, Gelman SE, Son JL, Pease ME, Quigley HA. Differential susceptibility to experimental glaucoma among 3 mouse strains using bead and viscoelastic injection. *Exp Eye Res*. 2010;91:415–424.

23. Steinhart MR, Cone-Kimball E, Nguyen C, et al. Susceptibility to glaucoma damage related to age and connective tissue mutations in mice. *Exp Eye Res*. 2014;119:54–60.
24. Coudrillier B, Pijanka J, Jefferys J, et al. Collagen structure and mechanical properties of the human sclera: analysis for the effects of age. *J Biomech Eng*. 2015;137:041006.
25. Murienne BJ, Chen ML, Quigley HA, Nguyen TD. The contribution of glycosaminoglycans to the mechanical behaviour of the posterior human sclera. *J R Soc Interface*. 2016;13:20160367.
26. Midgett DE, Jefferys JL, Quigley HA, Nguyen TD. The contribution of sulfated glycosaminoglycans to the inflation response of the human optic nerve head. *Invest Ophthalmol Vis Sci*. 2018;59:3144–3154.
27. Nguyen C, Cone FE, Nguyen TD, et al. Studies of scleral biomechanical behavior related to susceptibility for retinal ganglion cell loss in experimental mouse glaucoma. *Invest Ophthalmol Vis Sci*. 2013;54:1767–1780.
28. Cone-Kimball E, Nguyen C, Oglesby EN, Pease ME, Steinhart MR, Quigley HA. Scleral structural alterations associated with chronic experimental intraocular pressure elevation in mice. *Mol Vis*. 2013;19:2023–2039.
29. Leske MC. Open-angle glaucoma: an epidemiologic overview. *Ophthalmic Epidemiol*. 2007;14:166–172.
30. Kimball EC, Nguyen C, Steinhart MR, et al. Experimental scleral cross-linking increases glaucoma damage in a mouse model. *Exp Eye Res*. 2014;128:129–140.
31. Quigley HA, Cone FE. Development of diagnostic and treatment strategies for glaucoma through understanding and modification of scleral and lamina cribrosa connective tissue. *Cell Tissue Res*. 2013;353:231–244.

Investigative Ophthalmology & Visual Science